Journal of the European Ceramic Society 22 (2002) 1257–1262

www.elsevier.com/locate/jeurceramsoc

Crystalline structure and electrical properties of $YCo_xMn_{1-x}O_3$ solid solutions

D. Gutierrez[a], O. Peña[b], P. Duran[a], C. Moure[a,*]

[a]*Instituto de Ceramica y Vidrio, CSIC, Electroceramics Department, 28500 Arganda, Madrid, Spain*
[b]*LCSIM/UMR6511-CNRS, Université de Rennes I, Rennes, France*

Received 21 May 2001; accepted 6 August 2001

Abstract

Solid solutions corresponding to $YCo_xMn_{1-x}O_3$ system with $x=0.2...0.7$ have been studied. The powders were prepared by solid state reaction of corresponding oxides. Sintered bodies were obtained firing between 1250 and 1350 °C. The incorporation of 25 at.% of Co in the Yttrium manganite induced the appearance of a perovskite-type phase with orthorhombic symmetry and Space Group Pbnm. This feature was extended at least up to an amount of 70 at.% of Co. The increase of the Co content from 25 to 70 at.% led to a monotonic decrease of the orthorhombicity factor b/a. Electrical measurements have shown a semiconducting behaviour for all solid solutions with the perovskite-type structure. The room temperature conductivity increased with Co until the 33 at.% of Co, and then decreased. The 60/40 Co/Mn composition showed an increase of the electrical conductivity in comparison to the 50/50 composition and a corresponding decrease of the activation energy. Small polaron hopping mechanism is supposed to control the conductivity.

Keywords: Crystal structure; Electrical conductivity; Perovskites; $Y(Co,Mn)O_3$

1. Introduction

The Rare Earth manganites have focused a great interest because of their electrical and magnetic properties such as: semiconducting behaviour and magnetoresistive features. The most of the work has been devoted to the study of the properties of light RE manganites, particularly the $LaMnO_3$ compounds modified with Ba, Sr, or Ca.[1,2] The use of these solid solutions as ceramic electrodes for Solid oxide fuel cells (SOFC's) has been studied for several years.[3] More recently, the colossal magnetoresistive effect found in both single crystals and ceramic have been extensively treated by many authors.[4]

The light RE manganites crystallise with a perovskite-type structure and Space Group Pbnm. The crystalline lattice tends to increase its anisotropy, from rhombohedral, quasi-cubic symmetry for La, to orthorhombic symmetry, with high b/a ratio for Dy manganite, when the at. weight of the RE rises, and their ionic radii decrease. From the Er manganite, including Y, the RE manganites crystallise with a hexagonal symmetry and Space Group $P6_3cm$[5] in spite of the corresponding values of the Goldschmidt tolerance factor, $\mathbf{t}=(r_A+r_O)/(r_B+r_O)*\sqrt{2}$, for the perovskite-type structure. The structural change from perovskite-type to hexagonal symmetry can be associated, not only to the decrease of the tolerance factor, but also to the presence of a Jahn–Teller-type Mn^{3+} cation on B sites with octahedral coordination. Such cation promotes a strong anisotropic deformation, which induces the change of symmetry when the tolerance factor attains small enough value.[6] On the contrary, the heavy RE ferrites, such as the $ErFeO_3$ with the same tolerance factor, as 0.80 crystallises with an orthorhombic perovskite-type structure.

$YMnO_3$ is a ferroelectric, antiferromagnetic compound with a very low value of electrical conductivity[7]. At high voltages it shows a peculiar non-ohmic behaviour.[8] The solid solutions with the $CaMnO_3$ perovskite show a transition to an orthorhombic perovskite-type structure for an amount of approximately 22 at.% of Ca.[9] Similar behaviour was noticed when the Ni cation substitutes for Mn cations. In this case, 20 at.% of Ni is enough to change the structure from hexagonal $YMnO_3$-type to perovskite-type structure. A solid solution limit was

* Corresponding author. Tel.: +349-1-871-1800; fax: +349-1-870-0550.
E-mail address: cmoure@icv.csic.es (C. Moure).

0955-2219/02/$ - see front matter
PII: S0955-2219(01)00449-6

established for Ni amounts of 50 at.%, at difference of the 22–100% compositional range of solid solutions between $YMnO_3$ and $CaMnO_3$. Both solid solution types, $(Y,Ca)MnO_3$ and $Y(Ni,Mn)O_3$ are semiconducting compounds. In relation to the electrical conductivity behaviour, there is a difference between the systems. Whereas in the $(Ca,Y)MnO_3$ system the electrical conductivity increases monotonically with the Ca content, in the $Y(Ni,Mn)O_3$ system first increases up to an amount of 33 at.% Ni and after decreases for higher Ni amounts. The solid solution limit and the electrical behaviour of the $Y(Ni,Mn)O_3$ system was attributed to the high stability of the valence $2+$ of the Ni ion.[10]

$YCoO_3$ compound crystallises with a perovskite-type structure and an orthorhombic cell with Space Group Pbnm. This compound is synthesised at high pressures or in the presence of strongly oxidant cations, such as K^+. The crystallised perovskite has an yttrium-deficient structure.[11]

The aim of the present work is to study the effect of the incorporation of the Co cation which shows two stable valence values, (II) and (III), on the structure, symmetry and electrical properties of the $Y(Co,Mn)O_3$ solid solution.

2. Experimental methods

$Y(Co_xMn_{1-x})O_3$ compositions with $x = 0.10$–0.70 were prepared by solid state reaction of stoichiometric mixtures of reagent grade MnO, CoO and Y_2O_3 with submicronic particle size. The mixtures were homogenised in a ball mill using isopropanol. The dried mixtures were calcined at 1000 °C for 2 h. The calcined samples were milled again using the same technique, then dried, granulated, and uniaxially pressed. Granulometric analysis were carried out on the synthesised powders by means of laser counting, (Mastersizer model, Malvern Instruments, Ltd, UK) and BET techniques, (Quantachrome MS-16 model, Syosset, NY). Pressed pellets were sintered between 1250 and 1350 °C for several cycles. Apparent density was measured by water displacement. XRD analysis was performed both on the calcined powder and on the sintered samples using a D-5000 Siemens Diffractometer with CuK_α radiation. The phases were identified using a scanning rate of 2° 2θ/min, and the lattice parameters were calculated from the spectra obtained on the sintered samples using a scanning rate of $\frac{1}{2}^\circ$ 2θ/min. Si powder was employed as an internal standard. The microstructure of the sintered ceramics was observed by Scanning Electron Microscopy (SEM), (Zeiss DSM 950, Oberkochem, Germany) on polished and thermally etched surfaces. Four-point DC conductivity measurements were carried out for all the solid solutions with perovskite-type structure between 25 and 700 °C. Bar-shaped samples were painted with silver paste and fired at 800 °C for 1 h. For the electrical measurements, a Constant Current DC power supply (Tektronix, model PS280) and a HP Multimeter (model 44201[a]), with 1 μA DC current resolution was used. Activation energies were calculated from the corresponding Arrhenius plots. The ρ-T curves were reported to determine the NTC thermistor parameters. The Seebeck-Coefficient measurements were made on cylindrical samples (diameter of 0.3 cm and height of 1.5 cm) using a conventional technique for a rapid and qualitative determination of the majority charge-carrier sign.[12] For the measurements, two metal blocks containing the thermocouples held the sample. A heater on one block produced the temperature gradient in the sample. The thermoelectric voltage was measured between the same reference points.

The Goldschmidt tolerance factor, **t,** has been calculated using the ionic radii tabulated by Shannon,[13] taking into account the oxygen co-ordination number of the cations and the existence of different valence states of the Mn and Co cations, with different ionic radii, in the solid solutions. Mean ionic radius on B lattice sites has been used when two or more cations are present on that site.

3. Results

The apparent particle size, as measured by laser counting, was 2.2 μm, but this size corresponds to that of aggregates. The BET measurements indicated specific surface area values of 4.2 m^2/g, which is in agreement with an average particle size of 0.21 μm.

Table 1 summarises some results of the apparent relative density of sintered ceramics. The relative values have been referred to the theoretical density, D_{th} that has been calculated from the measured lattice parameters using the chemical formula $Y(Co_xMn_{1-x})O_3$ for different x values. Possible deviations from the oxygen stoichiometry have not taken into account for this calculation.

Fig. 1 shows the microstructure of two selected samples. The microstructure is slightly bimodal, with large and small grains, all of them in the microscale size

Table 1
Relative density of ceramics sintered in air at several temperatures

At.% Co	D_r (%) 1300 °C 2 h	D_r (%) 1325 °C 2 h	D_r (%) 1350 °C 2 h
0.25		95.4	95.2
0.30	95.2	96.3	
0.33	97.0	94.8	89.2
0.40	94.9	91.4	92.7
0.50	95.0	93.5	97.5
0.60	94.3	99.2	99.5

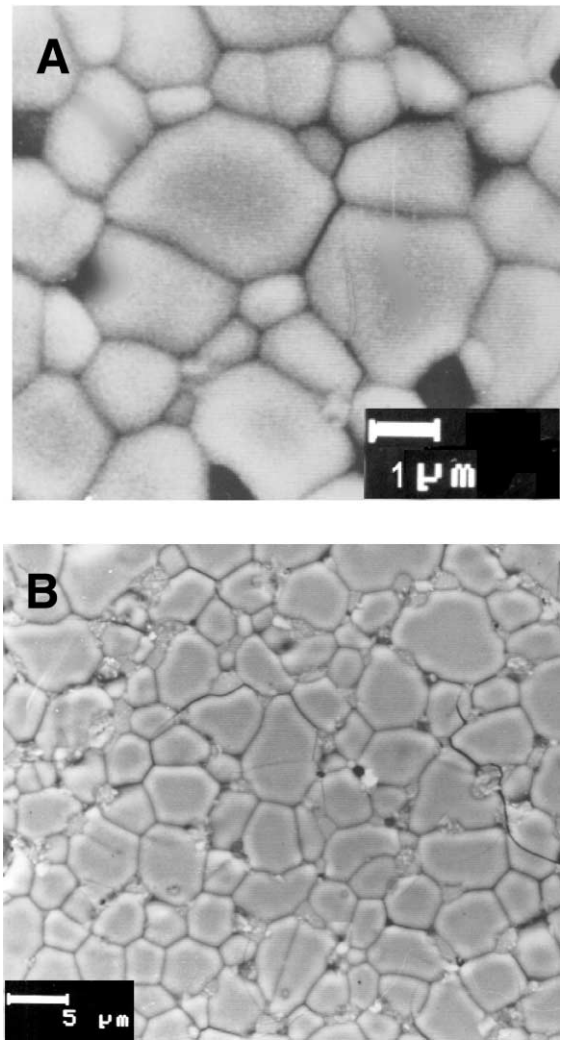

Fig. 1. Micrograph of polished and thermally etched surface of samples corresponding to (A) $x = 0.30$ and (B) $x = 0.60$, sintered at 1350 °C for 2 h.

range. The porosity is low as indicated by the measured relative density.

Fig. 2 shows the XRD patterns of samples with $x = 0.20$, 0.40 and 0.60. The spectra were indexed on a perovskite-type unit cell with space group Pbnm, in a similar manner to that of $Y(Ni,Mn)O_3$. As can be seen, perovskite phase has been formed in all cases, including that corresponding to $x = 0.60$. For $x = 0.2$, some amount of pure $YMnO_3$ is still present. Fig. 3 displays the XRD patterns of samples corresponding to the $YCo_{0.60}Mn_{0.40}O_3$ composition, fired under different thermal and atmospheric conditions.

Table 2 shows the measured lattice parameters of the solid solutions. The incorporation of Co cations causes a strong decrease of the b parameter, and a slight decrease of the a parameter. As a consequence, the orthorhombicity parameter b/a decreases. There is also a progressive decrease of the lattice volume i.e. the compactness grade of the perovskite lattice rises. As a

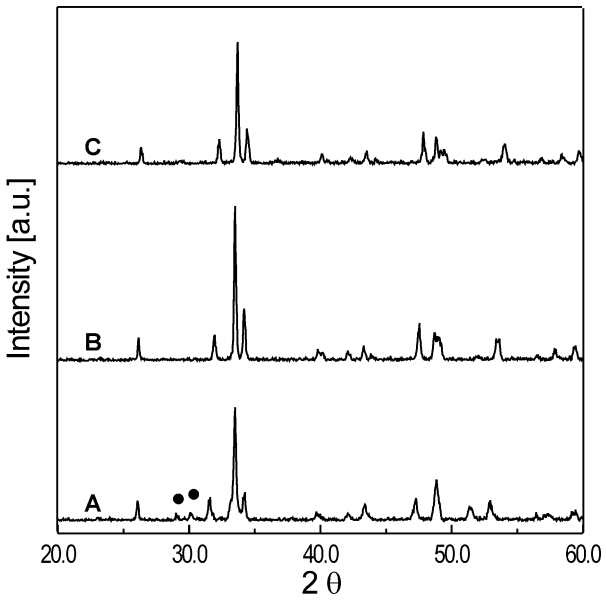

Fig. 2. XRD patterns of the solid solutions corresponding to samples with (A) 20, (B) 40 and (C) 60 at.% of Co. • $YMnO_3$.

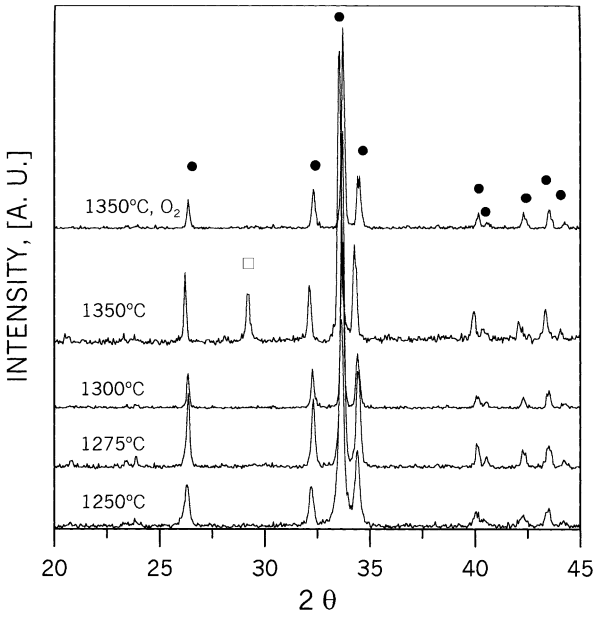

Fig. 3. XRD patterns of composition $YCo_{0.60}Mn_{0.40}O_3$ fired at different temperatures and atmospheres. •, $YCo_{0.60}Mn_{0.40}O_3$, □, Y_2O_3.

consequence, an increase of the theoretical density occurs. The perovskite lattice is, in all the cases, of type $a < c/\sqrt{2} < b$, i.e. O-type orthorhombic lattice.[14]

Fig. 4 shows the evolution of the tolerance factor, **t**, in function of the Co amount. For comparison, the evolution of **t** in the system $Y(Ni,Mn)O_3$ is also represented.

Fig. 5 depicts the Arrhenius plots of σT as a function of $1/T$. Table 3 shows the room temperature conductivity and the activation energy of all the samples. According to the obtained results, the conduction mechanism is a small polaron hopping thermally activated. Fig. 5 shows

Table 2
Lattice parameters of the solid solution $Y(Co_xMn_{1-x})O_3$

At.% Co	25	30	33	40	50	60	70
a (nm) ($\pm$0.0001)	0.5247	0.5245	0.5236	0.5245	0.5241	0.5229	0.5210
b ($\pm$0.0001)	0.5677	0.5654	0.5640	0.5618	0.5594	0.5565	0.5536
c ($\pm$0.0001)	0.7452	0.7460	0.7468	0.7470	0.7468	0.7454	0.7424
b/a	1.0819	1.0779	1.0771	1.0711	1.0673	1.0642	1.0626
V (nm^3) ($\pm$0.0004)	0.2219	0.2212	0.2206	0.2201	0.2189	0.2169	0.2141

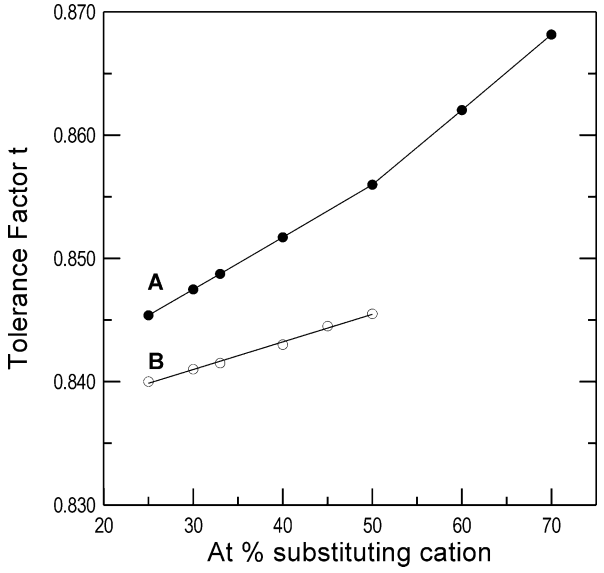

Fig. 4. Variation of tolerance factor **t** in function of substituting cation for (A) $YCo_xMn_{1-x}O_3$ solid solution, and (B) $YNi_x\ Mn_{1-x}O_3$ solid solution (taken from Ref. 10).

also the existence of a maximum in the conductivity for the sample with 33 at.% of Co. From this content, the conductivity decreases until the cation content of 50 at.% of Co. The sample with 60 at.% of Co shows an increase in the conductivity with respect to that of the sample with 50 at.% of Co. The electrical conductivity behaviour is similar to that described for the manganites with perovskite-type structure.[15]

Fig. 6 shows the Seebeck coefficient of the different solid solutions with perovskite-type structure. It can be seen that the majority carriers are holes for the whole compositional range. The Seebeck coefficient decreases when the Co amount increases, up to the x = 0.50 composition, but there is not sign change, such as was observed in the $Y(Ni,Mn)O_3$ system.[10] The composition $x = 0.60$ suffers a strong increase, indicating a possible new charge transport mechanism. Fig. 7 depicts the ρ-T curve of the 60/40 sample from 20 to 300 °C, and shows characteristic NTC behaviour.

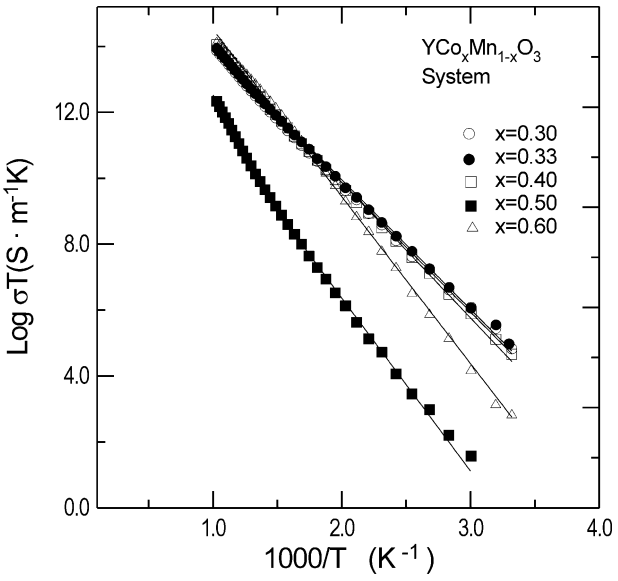

Fig. 5. Log σT vs $1/T$ for different compositions.

Table 3
Electrical conductivity at 25 °C and activation energy for the perovskite solid solution as a function of the Co amount

At.% Co	25	30	33	40	50	60
$\sigma_{25\ °C}$ (S m^{-1})	0.360	0.413	0.477	0.350	9.28E-3	5.78E-2
E_a (eV)	0.29	0.29	0.29	0.31	0.41	0.39

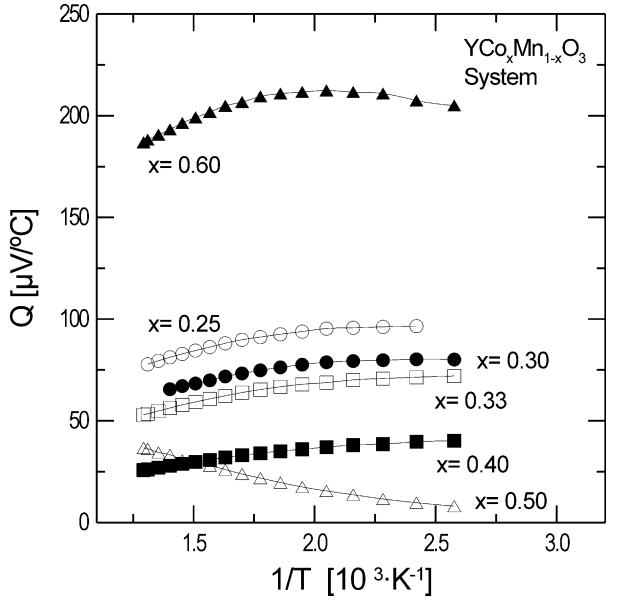

Fig. 6. Seebeck coefficient vs temperature for different solid solutions.

4. Discussion

The crystal-chemical behaviour of the samples containing less than 50 at.% of Co is very similar to that observed in the similar system $Y(Ni,Mn)O_3$.[10] The progressive disappearance of the Jahn-Teller cations,

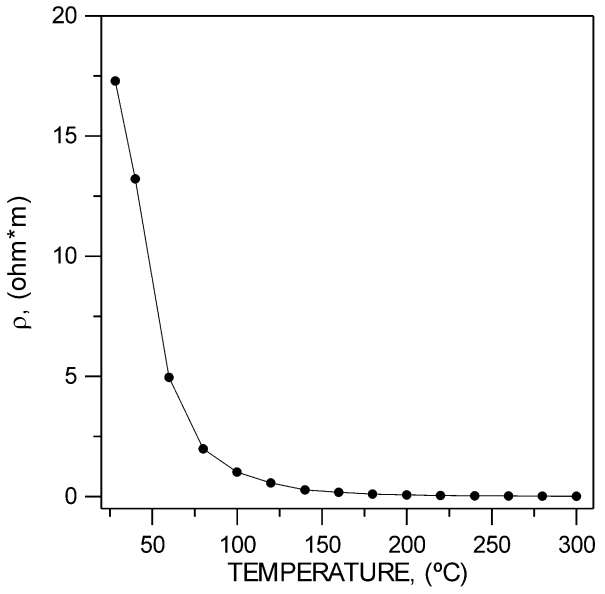

Fig. 7. Resistivity vs temperature curve for composition with $x = 0.60$.

Mn^{3+}, (which must adopt the 4+ valence state to preserve the valence equilibrium, because of the incorporation of lower-valence state cations such as the Co^{2+} cation), decreases the high anisotropy of the crystalline lattice, and promotes the appearance of a perovskite-type phase (see Fig. 2 and Table 2). When the Co-containing system is compared to the Ni-containing one, it can be seen that the amount of modifying cation needed to attain a single phase with perovskite-type structure is higher in the Co-containing system that in the Ni-containing one. The reason could be related to the possibility that a small amount of Co can adopt a trivalent state. As a consequence, the amount of Mn^{3+}, which is transformed to Mn^{4+} to attain the valence equilibrium, would be lower for the same amount of substituting cation. Therefore, one would expect that the transition from biphasic region to the single-phase region could be displaced towards a more Co-rich composition of the solid solution interval.

The same reason could explain the existence of the single-phase perovskite material for Co = 0.6, 0.7. Differently from the Ni-containing system, it is possible to claim the formation of a composition with the following valence distribution between the different cations:

$$Y[Co^{2+}_{1-x}Mn^{4+}_{1-x}Co^{3+}_{2x-1}]O_3 \quad (1)$$

or slight modifications around this equilibrium formula.

The formation of pure perovskite for Co higher than 50 at.% depends strongly on the thermal and atmospheric conditions. Fig. 3 shows the XRD patterns of samples fired at different temperatures, with a heating rate of 3 °C/min and a cooling rate of 0.5 °C/min, in air. A pattern corresponding to a sample fired in oxygen atmosphere, and cooling at 2 °C/min is also shown. As can be seen, the increase of the sintering temperature, from 1250 to 1350 °C leads to the appearance of an appreciable amount of yttria phase. On the other hand, the firing in O_2 atmosphere leads to a single phase, even at 1350 °C, (the same sintering in air leads to a biphasic sample). A more complete study of this behaviour is still in progress.

When the lattice parameters of the solid solutions containing Co are compared with those containing Ni, it is possible to see that the parameters of the former are slightly lower. It is thus reasonable to suppose that the Co cations are in the Low Spin state, for which the ionic radius is smaller than that of Ni^{2+}, (0.79 vs 0.83 Å, respectively).

The tolerance factor, **t** as a function of the Co content, shows, in Fig. 4, a faster increase compared to that of the $Y(Ni,Mn)O_3$ solid solution. For Co concentrations higher than 50 at.%, the rate is even higher. This behaviour is well correlated with the lower values of the orthorhombicity factor, b/a, observed in this system. The reason for this behaviour is the lower value of the ionic radius of Co^{3+} in the LS state, (0.665 Å) compared to Mn^{3+} (0.785 Å), and Mn^{4+} (0.68 Å). This feature leads to a more symmetric lattice.

The conductivity behaviour correlates well with the crystalline results. The progressive substitution of Co^{2+} for Mn^{3+} cations leads to an initial increase of the electrical conductivity until an amount of $x = 0.33$. followed for a decrease when $x > 0.33$. The model is similar to that applied in the Ni-containing system to explain the same behaviour.[10] According to this model, the Co^{2+} would not contribute to the conduction mechanism, because of the lack of another valence state of Co in the nearest neighbour sites. The only pair contributing to a controlled valence mechanism would be the Mn^{3+}–Mn^{4+} pair. It is easy to see that the number of these possible pairs increases until a content of 33/67 Co/Mn is reached. A subsequent rise in the Co percentage leads to a decrease in the concentration of possible pairs. It is possible to form 0.33 pairs per formula unit in the 33/67 compositions, whereas it is possible to form only 0.2 in the 40/60 composition, and 0.1 in the 45/55 one. This variation in the relative percentage between the two possible Mn cations explains the existence of a maximum in the conductivity values at an intermediate value of x, and the subsequent decrease up to the 50 at.% of Co.

According to formula (1), for $x = 0.6$ a new mechanism of charge transport between localised sites Co^{2+}, Co^{3+} can appear and contribute to an increase in the conductivity in comparison to the 50/50 composition. Actually, it is possible to suppose that a small amount of Co is in the valence state (III), which have the effect of maintaining equivalent amounts of Mn(III) in the solid solutions with $x \leqslant 0.50$. This fact would explain the

Table 4
NTC characteristic parameters of the solid solution $YCo_{0.60}Mn_{0.40}O_3$

Composition	ρ(Ω*m), at 25 °C	B (K)	α (%/K), at 25 °C
$YCo_{0.60}Mn_{0.40}O_3$	28	5065	−5.70

relatively high value of the conductivity for the 50/50 composition, in which formally there is not charge transfer between the same cations with different valence state.

The results obtained from the measurement of the Seebeck coefficient could support the above contention. The Seebeck coefficients of the different solid solutions correspond to positive carrier semiconductors, and no sign change is observed when the Co amount is higher than $x = 1/3$. This behaviour is different of that observed in the Ni-modified $YMnO_3$ solid solutions.[10] On the other hand, as has been established from the conductivity behaviour, an increase in the Co contents above $x = 1/3$ leads to a decrease in the conductivity value. To explain both facts it can be supposed that the Mn^{4+} cation is not the predominant in the solid solutions with $x > 1/3$, and therefore, some Co cations must adopt the $+3$ valence state to maintain the valence equilibrium, thus contributing to the conduction mechanism by supplying hole carriers between nearest neighbours Co^{2+} and Co^{3+}, Co^{3+} being the minority cation.

Fig. 7 displays the ρ-T curve corresponding to the 60 at.% Co solid solution, from which the NTC parameters have been calculated. The curve shows typical behaviour for NTC thermistors. Table 4 shows the calculated parameters. As can be seen, the composition shows a good Negative Temperature Coefficient. The sample has a B value higher than 5000, and an $\alpha = -5.7\%/K$, which makes this ceramic material very interesting for NTC applications, when compared with commercial compositions.[16]

5. Conclusions

The substitution of Co^{2+} for Mn^{3+} in the hexagonal $YMnO_3$ compound leads to a phase transition from hexagonal to orthorhombic, perovskite-type phase for Co amounts around 25 at.% in a similar manner to that reported for the $Y(Ni,Mn)O_3$ solid solutions. The reason for this transition seems to be related to the decrease of the Mn^{3+} Jahn–Teller cation concentration in the lattice. Above 50 at.% of Co, a solid solution is also formed, and a single-phase perovskite-type structure is developed. The single-phase formation depends strongly on the thermal history and atmospheric environment.

The perovskite-type solid solutions, ($x = 0.25$–0.60) are semiconducting materials. The conduction mechanism is due to small polaron hopping thermally activated. They show good values of electrical conductivity and promising NTC features.

Acknowledgements

This work was supported by Spain CICYT-MAT-97-0679-C02-01

References

1. Hammouche, A., Siebert, E. and Hammou, A., Crystallographic, thermal and electrochemical properties of the system $La_{1-x}Sr_xMnO_3$ for high temperature solid oxide fuel cells. *Mater. Res. Bull.*, 1989, **24**, 367–380.
2. Tanaka, J., Takahashi, K., Yukino, K. and Horiuchi, S., Electrical conduction of $(La_{0.8}Ca_{0.2})MnO_3$ with homogeneous ionic distribution. *Phys. Status Solidi*, 1983, **80**, 621–630.
3. Ostergard, M. J. L. and Mogensen, M., AC impedance study of the oxygen reduction mechanism on $La_xSr_{1-x}MnO_3$ in SOFC. *Electrochimica Acta*, 1993, **38**, 2015–2020.
4. Urishabara, A., Moritomo, Y., Arima, T., Asatmisu, A., Kido, G. and Yokura, Y., Insulator-metal transition and giant magnetoresistance in $La_{1-x}Sr_xMnO_3$. *Phys. Rew. B*, 1995, **51**(14), 103–109.
5. Muller, O. and Roy, R., *The Major Ternary Structural Families*. Springer, New York, 1974 pp. 357–358.
6. Yakel, H. L., Koehler, W. C., Bertaut, E. F. and Forrat, E. F., On the crystal structure of the manganese(III) trioxides of the heavy lanthanides and yttrium. *Acta Crys.*, 1963, **16**, 957–962.
7. Coure, Ph., Guinet, Ph., Peuzin, J., Buisson, G. and Bertaut, E. F., Ferroelectric properties of hexagonal orthomanganites of yttrium and rare earths. *Proc. Int. Meeting Ferroelectricity*, 1966, **V**, 332–340.
8. Moure, C., Fernandez, J. F., Villegas, M. and Duran, P., Non-Ohmic Behaviour and Switching phenomena in $YMnO_3$- based ceramic materials. *J. Eur. Ceram. Soc.*, 1999, **19**, 131–137.
9. Moure, C., Fernandez, J. F., Villegas, M., Tartaj, J. M. and Duran, P., Phase transition and electrical conductivity in the system $YMnO_3$–$CaMnO_3$. *J. Mater. Sci.*, 1999, **34**, 2565–2568.
10. Gutierrez, D., Peña, O., Duran, P. and Moure, C. Crystal structure, electrical conductivity and seebeck coefficient of $Y(Ni,Mn)O_3$ solid solution. *J. Eur. Ceram. Soc.*, in press.
11. Mehta, A., Berliner, R. and Smith, R. W., The structure of Yttrium cobaltate from neutron diffraction. *J. Solid State Chem.*, 1997, **130**, 192–198.
12. Heikes, R. and Ure, R., *Thermoelectricity: Science and Engineering*. Interscience Publishers, New York, 1961 pp. 311–322.
13. Shannon, R. D., Revised Effective Ionic radii and systematic studies of interatomic distanced in halides and chalcogenides. *Acta Cryst.*, 1976, **A32**, 751–767.
14. Pollert, E., Kupricka, S. and Kuzmisova, E., Structural study of $Pr_{1-x}Ca_xMnO_3$ and $Y_{1-x}Ca_xMnO_3$. *J. Phys. Chem. Solids*, 1982, **43**, 1137.
15. Subba Rao, G. V., Wanklyn, B. M. and Rao, C. N. R., Electrical transpor in rare-earth ortho-chromites, -manganites and ferrites. *J. Phys. Chem. Solids*, 1971, **32**, 345–358.
16. Moulson, A. J. and Herbert, J., *M., Electroceramics, Materials, Properties, Aplications*. Chapman & Hall, London, UK, 1990 pp. 140.